^{124}I in Differentiated Thyroid Cancer

103

Douglas Van Nostrand, Robert Hobbs, Frank B. Atkins, and George Sgouros

Introduction

^{124}I was first used in 1960 by Phillips et al. [1] for the treatment of differentiated thyroid carcinoma (DTC). However, because the decay of ^{131}I was more suited for therapy and its production was easier and less expensive than ^{124}I, ^{131}I has remained the most frequently used radioiodine isotope for the treatment of DTC. Likewise, because the decay characteristics of ^{131}I were more suitable for the imaging equipment at that time, ^{131}I became the most frequently used radioiodine isotope for diagnostic imaging of the thyroid. Subsequently, ^{123}I became available in the mid-1960s [2], and in the United States ^{123}I is now the most frequently used radioisotope of iodine for diagnostic imaging in differentiated thyroid carcinoma (DTC).

However, with the increased availability of cyclotrons, a few medical facilities in several countries and several commercial companies in the United States have begun producing ^{124}I, and with the availability of positron emission tomography (PET) scanners, which are the preferred imaging devices, several of these facilities have initiated studies to evaluate ^{124}I for both imaging and dosimetry in DTC.

Initial results suggest significant potential of ^{124}I for imaging and dosimetry, and this chapter reviews the production, decay, radiopharmacokinetics, advantages, disadvantages, lesion detection, dosimetry, and other studies using ^{124}I. The chapter concludes with a discussion of the future utility of ^{124}I imaging in DTC.

D. Van Nostrand, MD, FACP, FACNM (✉)
Nuclear Medicine Research, MedStar Research Institute and Washington Hospital Center, Georgetown University School of Medicine, Washington Hospital Center, 110 Irving Street, N.W., Suite GB 60F, Washington, DC 20010, USA
e-mail: douglasvannostrand@gmail.com

R. Hobbs, PhD
Department of Radiation Oncology, Johns Hopkins University, School of Medicine, Baltimore, MD, USA

F.B. Atkins, PhD
Division of Nuclear Medicine, MedStar Washington Hospital Center, Georgetown University School of Medicine, Washington, DC, USA

G. Sgouros, PhD
Department of Radiology and Radiological Science, Johns Hopkins University, School of Medicine, Baltimore, MD, USA

Production, Decay, and Radiopharmacokinetics of Radioiodine: The Basics

Isotopes of Iodine

Iodine is the 53rd element in the periodic table, which means that every atom of the element iodine contains 53 protons. However, there are a number of isotopes of iodine, which differ from each other only in the number of neutrons within the nucleus. Although their atomic masses (i.e., sum of the protons and neutrons) are different, biochemically all of these various isotopes of iodine behave identically. In fact, over 35 different isotopes of iodine have been identified, and their physical properties have been well characterized. However, among all of these isotopes, only one isotope of iodine, namely, ^{127}I, is stable. Consequently, this is the only form of iodine that can be found to occur naturally in our environment. All of the other isotopes of iodine undergo a nuclear transformation over some time interval and in the process convert into an isotope of a different element, which in turn may or may not be stable.

The number (mass number) that is associated with the chemical symbol "*I*" represents the number of neutrons in the nucleus of that particular isotope of iodine plus the element number (i.e., 53). Any isotope of iodine with a value less than 127 would therefore have fewer neutrons than the

L. Wartofsky, D. Van Nostrand (eds.), *Thyroid Cancer*, DOI 10.1007/978-1-4939-3314-3_103

stable form of iodine. Likewise, higher values would indicate more neutrons.

Half-Life

One way of expressing the instability of any radioactive isotope (radionuclide) is in terms of its physical half-life ($T_{1/2}$). This represents the average time interval required for half of the atoms of that radionuclide present at any instant in time to undergo a nuclear transformation into another element and is independent of the chemical and physical environment containing these radionuclides. More importantly, not only does the number of unstable atoms diminish over time at this rate but so does the *activity*, a quantity defined as the number of nuclear transformations per second. This is typically expressed in units of megabecquerels [MBq] or millicuries [mCi] and is proportional to the number of radioactive atoms present at that instant of time. After an elapsed time equal to $7 \times T_{1/2}$ (the half-life), less than 1 % of the initial activity will remain. The 35 known isotopes of iodine range from the lightest (^{108}I) to the heaviest (^{144}I). In general, the farther away the atomic number is from the value for the stable form of that element, the shorter is its half-life. As a consequence, all of the radioisotopes of iodine lighter than ^{120}I have half-lives <20 min, while those heavier than ^{133}I have half-lives <60 min with ^{135}I being an exception at $T_{1/2} = 6.6$ h. There is one radioactive isotope of iodine, namely, ^{129}I, which has a very long half-life (15.7 million years). With a few exceptions, those radioisotopes of iodine lighter than ^{127}I will transform into the preceding element in the periodic table (tellurium) while the heavier radioisotopes of iodine transform into the next higher element (xenon).

Radioactive Decay

In general, the most common mechanisms by which these unstable radionuclides transform (i.e., *decay*) depend on their weight relative to the stable configuration. In the case of radioisotopes of iodine, those isotopes that are lighter than ^{127}I decay by either *electron capture* (ec) or *positron* emission (β^+) and those that are heavier decay by electron (better known as beta) emission (β^-). Positrons (β^+) are special particles that are created during the nuclear transformation by some radionuclides. They have characteristics that are similar to the electrons found in all atoms with one main exception, namely, they carry a positive rather than a negative charge. As such, positrons are not a normal constituent of matter and in fact belong to a group referred to as "antimatter." The ultimate fate of this antiparticle after it is ejected from the nucleus is to slow down as it loses energy until it eventually can combine with its corresponding particle, namely, the electron. At this point in time, the antiparticle-particle combination cannot coexist and the two particles destroy (i.e., *annihilate*) each other with the simultaneous formation of two high-energy photons (511 keV gamma rays) that travel away from the point of annihilation in nearly opposite directions (opposite from the center of mass reference frame). It is this unique feature of all positron emitting radionuclides, including ^{124}I, that is exploited in PET imaging systems – namely, the simultaneous detection (coincidence) of two gamma rays of very specific energy originating from the same location that results in superior imaging capability over conventional gamma camera imaging. However, a discussion of ec, β^+, and $\beta-$ is beyond the scope of this chapter.

Choice of Radioiodine for Imaging, Dosimetry, and Therapy

Due to the preferential uptake of iodide (I^-) into thyroid epithelial cells by the sodium-iodide symporter (NIS), radioisotopes of iodine have played an important role in the diagnosis and treatment of benign and malignant thyroid diseases. The temporal aspects of the uptake and clearance of iodine within normal and metastatic thyroid tissue can be quite variable. Nevertheless, it is a relatively slow process in which the maximum concentration of an orally administered quantity of any of the radioisotopes of iodine may take 24 h or longer to achieve. Likewise, the release of the iodine from these cells occurs gradually over the course of several or more days. As a result of the relatively slow iodine biokinetics, (1) diagnostic imaging is generally more optimal when performed ~24–72 h after administration of the radioiodine, and (2) dosimetry studies to determine patient-specific prescribed activities of ^{131}I for therapeutic purposes typically require measurements to be performed over a minimum of 4 days. Consequently, short-lived (half-life <12 h) radioisotopes of iodine are not practical for the diagnosis and treatment of thyroid disease since very little radioactivity would still be present in the patient after a few days. Of all of the radioisotopes of iodine potentially available, only four meet the above characteristics and have been used as tracers and therapeutic agents in medicine (see Table 103.1). However, depending on its intended purpose, other characteristics of the radioiodine may either be a benefit or a detriment. For diagnostic imaging and dosimetry, a nuclear transformation that results in the production of gamma rays is beneficial because it is this form of radiation that allows localization, quantification, and subsequent kinetic analysis of the distribution of iodine within the patient. Two of these

Table 103.1 Physical decay characteristics of common radioisotopes of iodine used for medical applications

Radionuclide	Half-life	Decay mechanism
^{123}I	13.2 h	ec (100 %)
^{124}I	4.18 days	ec (76 %); β^+ (24 %)
^{125}I	59.4 days	ec (100 %)
^{131}I	8.02 days	β^-

radioiodines, namely, ^{123}I and ^{131}I, have gamma rays that can be imaged using conventional gamma cameras. The gamma rays that result from the annihilation of the positron emitted from ^{124}I also allows ^{124}I to be used for both imaging and dosimetry, but in this case a PET scanner is preferred. However, unless the energy of the gamma ray is sufficiently high enough to allow it to escape from the patient, it would not be useful for in vivo imaging, which is the case for ^{125}I. For therapy purposes, a nuclear transformation resulting in the release of a β particle is beneficial because the β particles may deposit a significant amount of energy, i.e., radiation absorbed dose, in the tissue that "takes up" and stores the radioiodine. This in turn results in a potential therapeutic effect. ^{131}I is typically used for therapies, but ^{124}I has also been considered for this application.

Iodine-124 (^{124}I)

^{124}I is a very promising radioisotope. It has a half-life of 4.18 days, which is sufficiently long enough to allow dosimetry to be performed. This radioisotope is also different from the other longer-lived isotopes of iodine in that it is a positron emitter (β^+), which means that diagnostic imaging can be performed using a PET scanner rather than a gamma camera. As a result there is a significant improvement in the overall quality of these images when compared to those of ^{131}I, as well as a more accurate, quantitative assessment of the uptake and clearance of iodine within both normal and metastatic tissues. The latter can then be used to predict the radiation absorbed dose to individual lesions that would be delivered from a subsequent therapeutic treatment of ^{131}I. Furthermore, most of the PET imaging devices today are hybrid PET/CT systems so that precise anatomical localization of the regions of radioiodine uptake can also be determined.

Unfortunately, some of the characteristics of the decay scheme of ^{124}I (Fig. 103.1) are less than ideal. To begin with, ^{124}I is not a pure β^+ emitter. Only 23.5 % of the decays actually result in positron emission, which means fewer annihilation photons that can be used for imaging. In addition, there is an abundance of high-energy gamma rays, which can potentially interfere with the imaging process. This is especially true for the 603 keV gamma rays that are emitted in cascade with the β^+ positrons. Fortunately, these can be

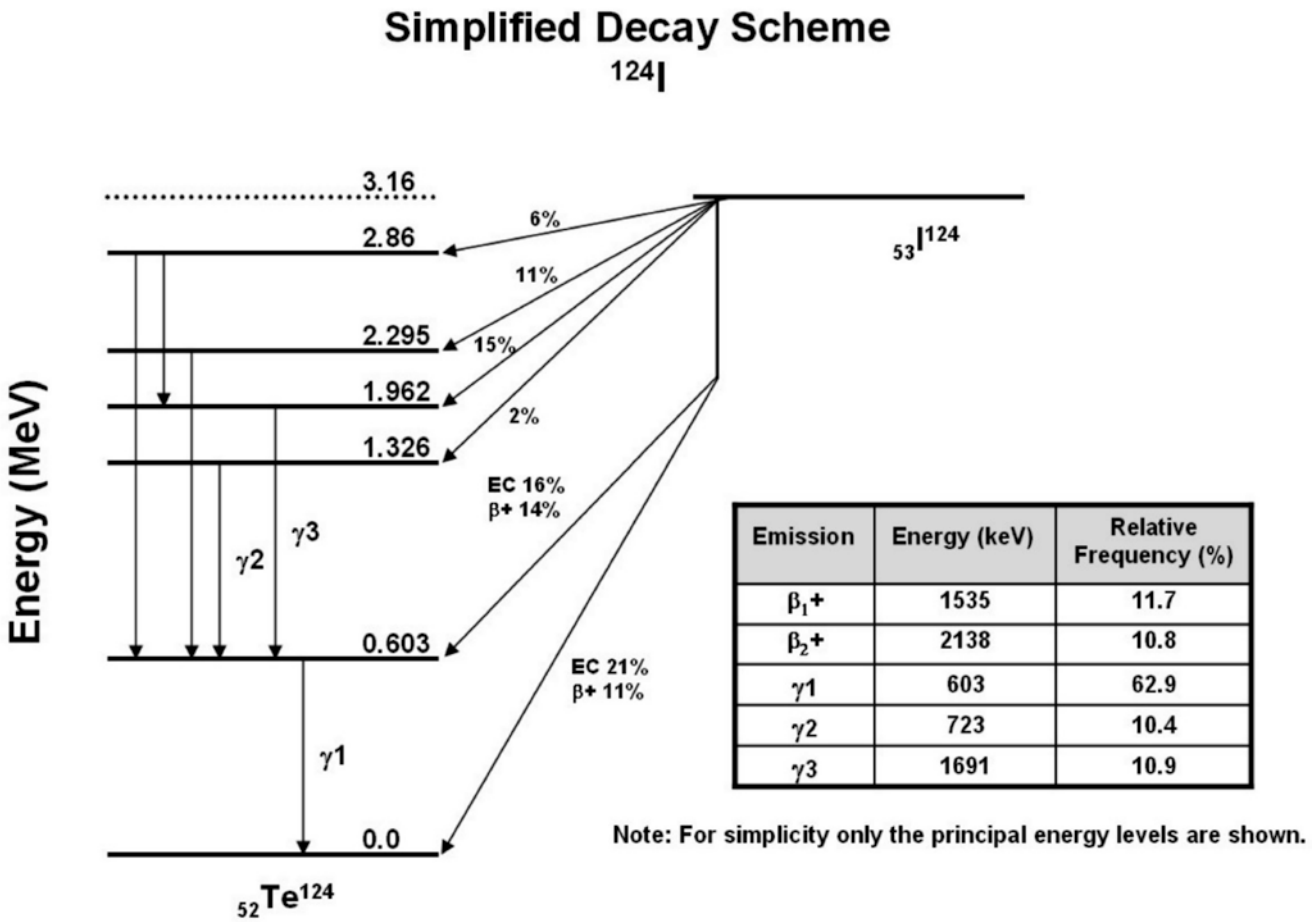

Fig. 103.1 This is a simplified decay scheme for ^{124}I listing the principal pathways for positron emission and electron capture and the nuclear energy levels for ^{124}Te

eliminated to a large extent by energy discrimination from the 511 keV annihilation photons, although a non-negligible fraction of 603 keV photons that have scattered and subsequently lost energy will still be detected in a narrow 511 keV window. Finally, the positrons themselves are ejected with a relatively high energy, which can also result in a degradation of image quality since the annihilation photons used to form the image will originate from a location a short distance away from the actual location of the ^{124}I atom – the higher the β^+ energy, the greater this distance. Despite these limitations, ^{124}I has been shown to produce high-quality, quantitative images using a PET imaging system at an acceptable radiation dose to a patient [3–8]. ^{124}I also has potential for its use as a therapeutic radionuclide, although cost and availability would be issues.

Radiopharmacokinetics

It is generally assumed that ^{124}I and ^{131}I are equivalent biokinetically, and this was confirmed in a study by Atkins et al. [9] who examined the clearance of oral administration in capsular form of both ^{131}I and ^{124}I from the blood compartment in a group of 22 patients with DTC (see Graph 103.1). In this study an effective half-life was determined for each patient based on a mono-exponential regression to both sets of clearance data. The average effective half-life in the blood compartment for the group (excluding the one patient noted) was 14.4±5.0 h for ^{124}I and 13.7±4.5 h for ^{131}I, which were not statistically different.

Production of ^{124}I

Due to the short half-life of ^{124}I, this is not a radionuclide that is found naturally occurring within the environment. Therefore, it must be artificially produced [10–12]. One common way in which a variety of medically useful radionuclides are produced, especially those that decay by positron emission, utilizes a cyclotron, an example of which is shown in Fig. 103.2.

This device is used to accelerate projectiles such as a beam of protons or deuterons (the name given to the bound state of a proton and a neutron) to sufficiently high energies such that they can enter the nucleus of a target atom at which they are directed. Often these collisions cause one or more constituents of the nucleus (i.e., protons and/or neutrons) to be ejected. As a result, the final nucleus could be a different element than that of the target. This process is often expressed using the following format: Target Nucleus (Incident

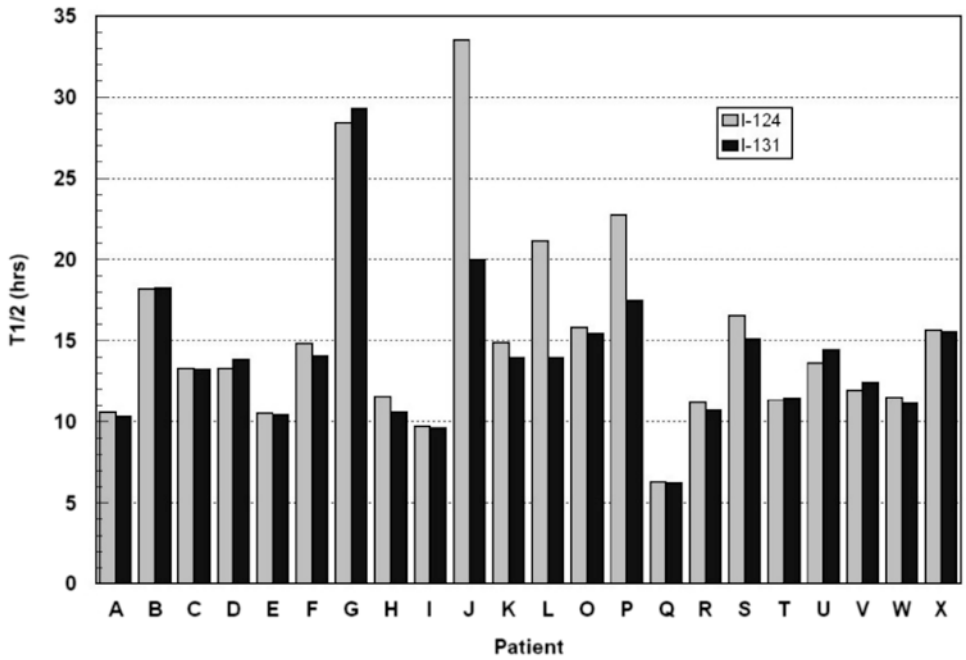

Graph 103.1 Effective half-life of ^{131}I in group of patients ($N=22$) with metastatic well-differentiated thyroid cancer who were studied using both ^{131}I and ^{124}I. The clearance data for ^{124}I was corrected for the different half-lives of the two radioisotopes of iodine. One patient (*J*) experienced complications due to his hypothyroid state and required admission to the hospital during the study. This probably accounts for the large discrepancy in this case, and this patient was excluded from the final analysis. Three other patients (not shown) were either for pre-ablation therapy or had extensive metastatic disease which resulted in an increasing or relatively flat clearance due to protein-bound radioiodine, which is not removed by renal excretion and hence could not be represented by a simple effective half-life measurement

Projectile, Ejected particles) Resulting Nucleus. For example, ^{111}In can be produced from the interaction ^{112}Cd (p,2n)^{111}In. In this case, high-energy protons bombard ^{112}Cd and remain in the nucleus while knocking out two neutrons. This results in the production of ^{111}In, the next element in the periodic table. Likewise, ^{124}I is a cyclotron-produced radionuclide. Various methods have been used to produce ^{124}I that employ different target materials, projectiles, and energies, some of which are listed in Table 103.2. The method highlighted in the table, namely, the (p,n) reaction on a $^{124}TeO_2$ target, is the approach used by IBA Molecular in the commercial production of ^{124}I. This method, while not providing the highest yield, does give the best radioiodine purity such that their Na^{124}I capsules contain <0.1 % impurities (unwanted radionuclides) of ^{125}I, ^{126}I, ^{130}I, and ^{131}I and <3 % impurities of ^{123}I. However, unlike iodine, which has only one stable isotope, Te (tellurium) has effectively eight stable isotopes, six of which are truly stable and the other two that have half-lives that are so long (>10^{18} years) that for practical purposes they can be considered as stable. Consequently, Te exists in nature in all of these elemental forms. If ^{130}Te, which is the most abundant isotope of tellurium, were to be bombarded by the same protons in the cyclotron, then ^{130}I could also be produced in the target along with ^{124}I. This would result in an unnecessary radiation dose to the patient. In order to minimize the production of other radioactive impurities, it is then necessary to first process the tellurium such that the amount of ^{124}Te present in the target has been substantially increased from its natural abundance of only 4.75 % to approximately 99.8 %. When used in this *highly enriched* ^{124}Te oxide form, the production of other radioisotopes of iodine can be kept at an acceptable level.

Fig. 103.2 Medical cyclotron *Cyclone 18/9* from IBA (Ion Beam Applications) capable of accelerating protons to 18 MeV in energy. Using a highly enriched (>99.9 %) $^{124}TeO_2$ target, a recovered activity of 50 mCi ^{124}I is possible after a 5 h irradiation (This image has been reproduced with permission from IBA (Ion Beam Applications)

Imaging Technique

When radionuclides, such as ^{123}I and ^{131}I, are imaged using gamma cameras (see Chap. 11), it requires collimators, image uniformity corrections, and window settings that are appropriate to the energy of the gamma ray(s) emitted by the particular radionuclide be used. Although the energy and relative abundance of the positrons that are emitted by β^+ radionuclides might be very different, they have a commonality in terms of the imaging. The photons used to generate these images are always the same, namely, the pair of 511 keV photons that are formed simultaneously by the annihilation of the positron with the electron and then travel in nearly opposite directions. However, the abundance and energy of prompt photons (gamma rays) that might accompany the β^+ decay do indeed depend on the particular isotope. From that standpoint, the decay scheme of ^{124}I includes a number of high-energy photons, unlike ^{18}F. The consequence of these extra photons is that they could in principal increase the number of false coincidences as measured by the detector; however, in practice, choosing a narrower rather than a wider energy range around the 511-keV photopeak decreases these false coincidences to near background level.

Table 103.2 Common methods of cyclotron production of ^{124}I [65]

Nuclear reaction	Effective energy (MeV)	Target material	Enrichment (%)	Yield (MBq/μAh)	Radioiodine impurities (%)
^{124}Te(p,n)^{124}I	13 → 9	Te	99.51	20	^{123}I(41)
	12.9 → 0	TeO_2	99.8	13	^{123}I(10.039), ^{125}I(0.018), ^{126}I(0.041), ^{130}I(0.379)
^{125}Te(p,2n)^{124}I	20.1 → 10.5	TeO_2	93	43.3	^{123}I(8), ^{125}I(5)
^{123}Te(d,n)^{124}I	15 → 8	Te	91.7	18.9	^{125}I(0.35), ^{126}I(0.39),^{131}I(0.08)

Advantages and Disadvantages

The advantages and disadvantages of ^{124}I are several as listed in Table 103.3. First, ^{124}I decays by positron emission. This, of course, allows ^{124}I to be imaged using a PET scanner resulting in (1) better contrast and spatial resolution, (2) 3D tomographic images, and (3) fusion of the tomographic images with computer tomographic images (CT) and/or magnetic resonance images (MRI). The capability to superimpose or fuse the PET images with the CT or MRI images is very important in helping to determine whether a region concentrating ^{124}I is located within a physiological structure, such as the salivary glands, gastrointestinal tract, and/or residual functioning thyroid tissue remnant or in a structure where iodine is not normally found, the latter suggesting metastatic thyroid cancer. ^{124}I PET imaging also allows superior lesion, organ, and whole-body dosimetry, which will be discussed in more detail later in this chapter. An additional advantage is that ^{124}I is relatively easy to produce in adequate quantities from available small medical cyclotrons, and finally, the radiochemistry of iodine is well established.

However, ^{124}I also has disadvantages (see Table 103.3). Until recently, the availability of ^{124}I was limited to only university-affiliated or research facilities that had a cyclotron and the resources to produce ^{124}I. At the time of the publication of this textbook, IBA Molecular Imaging is commercially manufacturing and distributing ^{124}I from a cyclotron in Richmond, Virginia. Unfortunately, ^{124}I is still not widely available, not approved by the Food and Drug Administration (FDA), expensive, and not approved for reimbursement by third-party payers in the United States. In addition, because the positron emitted from ^{124}I travels a slightly longer distance than a positron emitted from ^{18}F before colliding with an electron, the spatial resolution of ^{124}I is slightly worse than that of ^{18}F.

Table 103.3 Advantages and disadvantages of ^{124}I

Advantages
• Favorable half-life of 4.2 days
• As a result of coincidence PET imaging, improved special and contrast resolution relative to planar imaging
• Additional improved spatial resolution because of "time-of-flight" technology
• Tomographic images instead of planar images
• Fusion of PET tomographic images with CT and MR tomographic images resulting in improved specificity
• Lesion, organ, and whole-body dosimetry
• Easier production from small medical cyclotrons [66], which are becoming more widely available
• Established iodine radiochemistry
Disadvantages
• Availability
• Cost
• Not approved by the Food and Drug Administration
• Not reimbursed by third-party payers
• Slightly lower spatial resolution than ^{18}F

Lesion Detection

^{124}I may be used for superior detection and localization of sites of normal residual and/or functioning metastatic DTC.

Lesion Detection and Comparison with ^{131}I Planar Imaging

An excellent review was published by Freudenberg et al. [5] in 2011, and Freudenberg et al. [3], Phan et al. [6], Capocetti et al. [7], Van Nostrand et al. [8], and Khorjekar et al. [13] have reported the detection of sites of functioning normal residual thyroid tissue and/or metastases from differentiated thyroid cancer (see Graph 103.2). Each of these studies demonstrated overall better detection of functioning areas of normal thyroid tissue and/or metastatic disease secondary to differentiated thyroid cancer using ^{124}I PET and/or PET-CT compared to ^{131}I radioiodine planar scans, and the improved detection of metastases can be dramatic (see Figs. 103.3 and 103.4). Of note, the ^{131}I radioiodine planar scans performed by Freudenberg et al. [3], Phan et al. [6], and Capocetti et al. [7] were post-therapy ^{131}I scans. The reason for the variance in the number of patients with more lesions detected (not

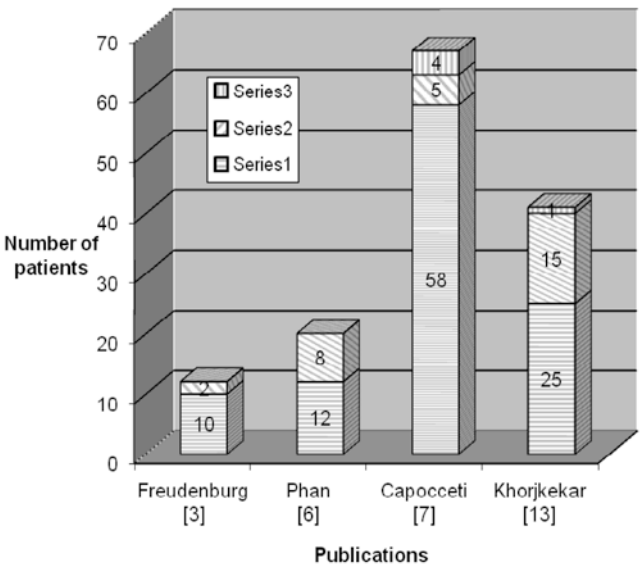

Graph 103.2 The *horizontal line* areas represent patients whose ^{124}I PET images were similar to the ^{131}I planar images. The *diagonal line* areas represents patients whose ^{124}I PET images detected more lesions than the ^{131}I planar images, and the *vertical line* areas represent patients whose ^{131}I planar images detected more lesions than ^{124}I PET images [3, 6, 7, 13]

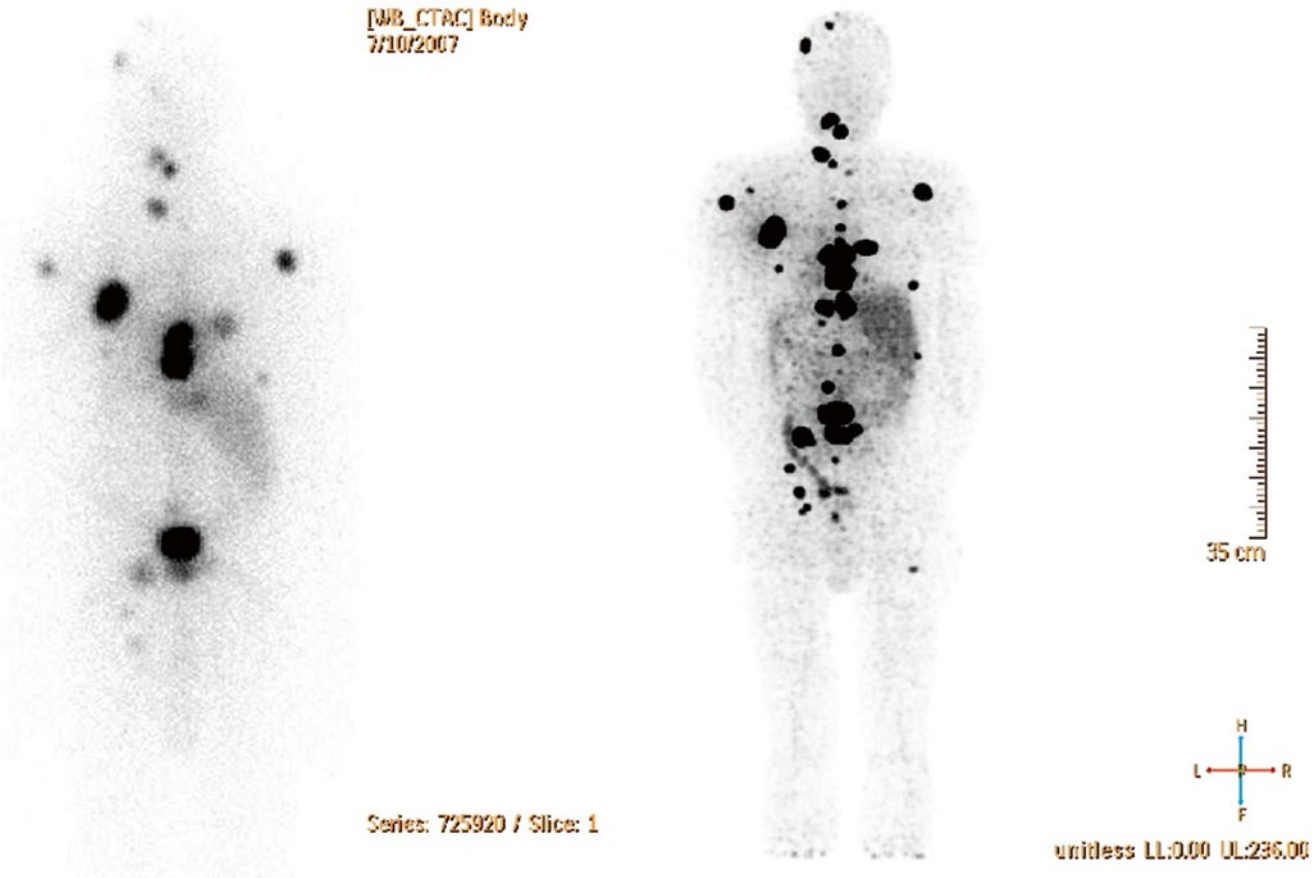

Fig. 103.3 Both of the above images were obtained in the same patient. The image on the *left* is a pre-therapy posterior planar ^{131}I whole body image demonstrating approximately 18 foci of ^{131}I uptake indicative of metastatic differentiated thyroid cancer. Although modest diffuse liver activity is present, this is not a post-therapy scan and this is not diffuse metastases. The image on the *right* is the posterior ^{124}I PET image from the maximum intensity projection (MIPS) demonstrating multiple additional foci of ^{124}I uptake suggesting metastatic differentiated thyroid cancer that were not detected on the ^{131}I images (This figure was originally published in Van Nostrand et al. [8]. Reproduced with permission from Mary Ann Liebert, Inc. Publishers)

shown) as well as the actual numbers of additional lesions detected most likely represents the different patient populations studied having higher and lower incidences of metastatic disease.

However, despite the improved detection of metastatic foci of DTC by ^{124}I PET scans, a new artifact has already been described. Fatah et al. [14] reported that areas of ^{124}I uptake near the trachea may result in annihilations of the positron occurring in the opposite wall of the trachea resulting in false-positive uptake of ^{124}I in that area. As noted earlier, the PET scanner does not image the positron; instead it forms an image using both of the 511 keV gamma rays that result from the annihilation of the positron with an electron. As a result, the annihilation may actually occur a small distance away from where the positron was actually emitted. In 17 % of the 29 patients that Fatah et al. [14] evaluated with ^{124}I PET/CT, this artifact, a so-called shine-through artifact, was observed with a relative intensity between 0.7 % and 14 % (see Fig. 103.5). Phantom experiments by this group also demonstrated the artifact nicely and showed that the effect decreases sharply as the thickness of the material between the activity and air cavity increases.

Comparison with SPECT-CT

To our knowledge, no data have been published comparing the lesion detection of ^{124}I PET scans to SPECT-CT scans using either ^{123}I or ^{131}I. Such a comparison is certainly warranted and encouraged. However, in addition to evaluating lesion detection, one must also consider cost, potential alteration of management, and if possible the impact on patient outcome. Although one might anticipate that the cost would be less for the ^{123}I or ^{131}I SPECT-CT scans, this may not be the case. A radioiodine SPECT-CT scan for one area of the body may take more time that an ^{124}I PET scan of the entire whole body. In addition, SPECT-CT scans of the entire whole body may be prohibitive from a time standpoint.

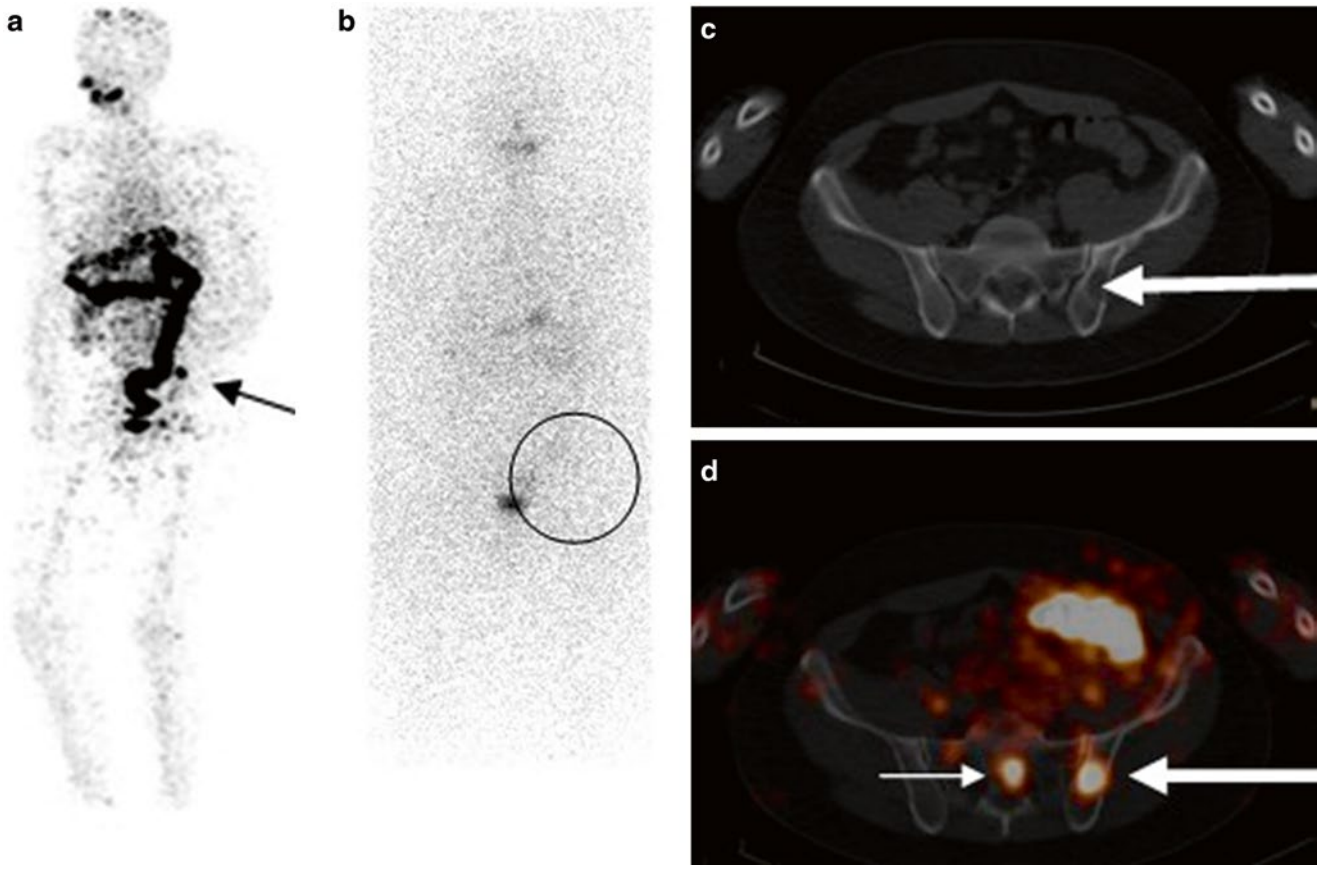

Fig. 103.4 The first image, (**a**), demonstrates a single projection of the ^{124}I PET MIPS image in the left anterior oblique position with an abnormal focus of uptake (*arrow*), and (**b**) demonstrates an anterior ^{131}I image in the same patient, which is completely normal. The posterior image was also normal. No planar LAO image was obtained. In image (**b**), a focus has been *circled* where the abnormality noted on the ^{124}I PET image should have been seen on the ^{131}I image. Image (**c**) is a transverse CT image of the pelvis demonstrating an abnormal lytic finding in the patient's left pelvic bone (*arrow*), which corresponds to the abnormal focus of uptake on the ^{124}I PET image noted in (**a**). Image (**d**) is the fusion of the transverse CT image of the pelvis with the corresponding transverse ^{124}I PET image (*color*), which demonstrates the utility of fusing the ^{124}I PET image with the CT image. The fused images demonstrate that the ^{124}I abnormal uptake (*reddish-yellow-white area*) corresponds precisely to the abnormality on the CT scan (*large white arrow*). In addition to the identification of this abnormality, the ^{124}I images demonstrate a second focus of abnormal ^{124}I uptake, which correlates with another abnormality in the sacrum on the CT image suggesting metastatic disease (*small white arrow*). In this patient, the ^{124}I PET scan identified at least three and possible four foci of radioiodine uptake that were not identified on the ^{131}I images. All these additional foci were suggestive of metastatic thyroid cancer (This figure was originally published in Van Nostrand et al. [8]. Reproduced with permission from Mary Ann Liebert, Inc. Publishers)

Comparison of ^{124}I PET-CT and ^{124}I PET-MR

Nagaraha et al. [15] compared the utility of intrinsically co-registered ^{124}I positron emission tomography (^{124}I PET) and computer tomography (CT) together designated as ^{124}I PET-CT with software co-registered ^{124}I PET and magnetic resonance imaging (MRI) together designated as ^{124}I PET-MR in 33 patients evaluated for thyroid remnant tissue and lymph node metastases in the neck. Patient-based analysis demonstrated that 26 of the 33 (79 %) patients had at least 1 lesion classified as thyroid tissue remnant based on the PET images only, but only 11 (42 %) and 16 (62 %) had any morphological correlation on CT and MRI, respectively. Twelve (36 %) patients had at least 1 lesion classified as lymph node on PET images alone, of which 9 (75 %) had a morphological correlation on both CT and MRI. For lesion-based analysis, ^{124}I PET identified a total of 61 lesions as thyroid remnant tissue, of which 16 (26 %) correlated with morphological findings on CT and 33 (54 %) on MRI, and a total of 29 (27 %) lesions as lymph nodes, of which 18 (62 %) correlated with morphological findings on CT and 24 (83 %) on MRI. A change of diagnosis using the combined ^{124}I PET-CT data occurred in eight patients and with ^{124}I PET-MRI in 10 patients. They concluded that ^{124}I PET-MRI was superior to ^{124}I PET-CT in the neck.

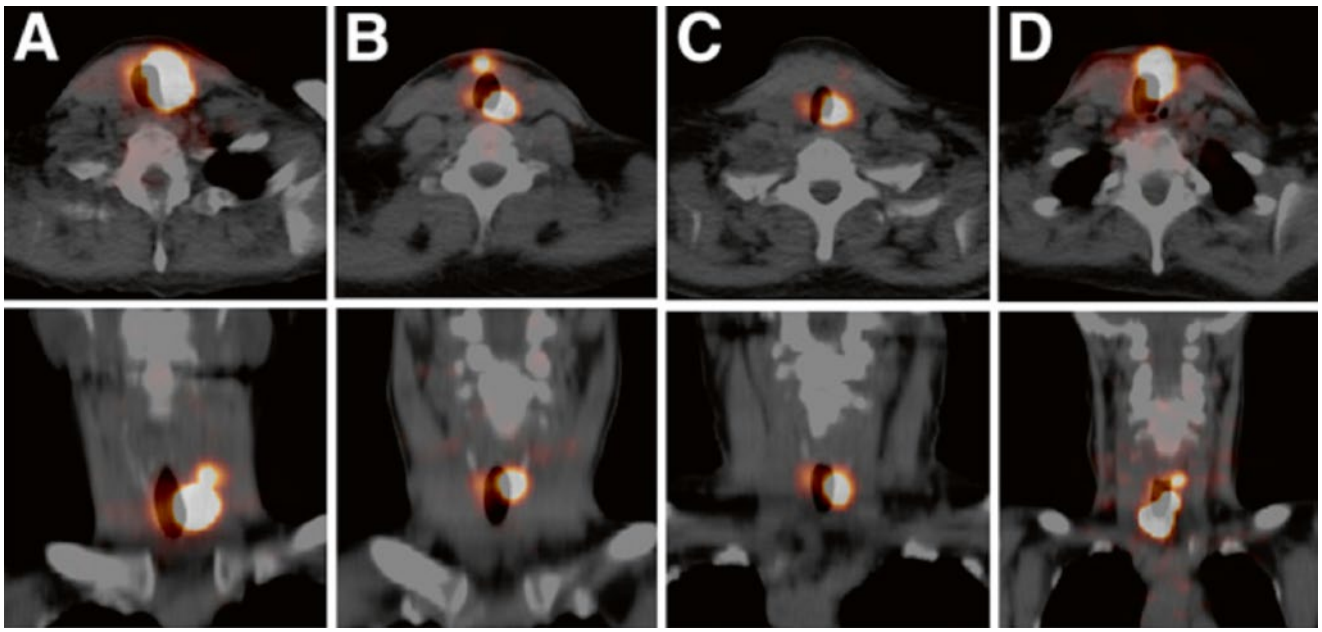

Fig. 103.5 These images from Fatah et al. [14] demonstrate shine-through in four patient studies at 96 h after oral intake of 20–25 MBq of ^{124}I. *Top row* shows transaxial PET/CT images; *bottom row*, coronal images. (**a**–**d**) represent four different patients with *top* level of viewing windows of 29 %, 4 %, 24 %, and 2 % of image maximum (This figure was originally published in *JNM*. Abdul-Fatah et al. [14]. © by the Society of Nuclear Medicine and Molecular Imaging, Inc.)

The Frequency of Positive ^{131}I Post-Therapy Scans in Patients Who Had a Negative ^{124}I Pre-Therapy Pet Scans and Were Treated with ^{131}I

In patients with a negative pre-therapy radioiodine scan and an elevated serum thyroglobulin level, treatment with ^{131}I is frequently referred to as a "blind treatment," and "blind treatments" are very controversial. One may argue that if one cannot visualize uptake on the pre-therapy scan, there will be no significant therapeutic effect. Alternatively, with decreasing amounts of prescribed activity used for the pre-therapy scan, a negative diagnostic radioiodine scan does not necessarily mean that a metastatic focus is non-radioiodine avid and that a therapeutic radiation absorbed dose cannot be delivered to that metastatic focus. In support of the potential beneficial effect from a "blind treatment," many authors have evaluated the frequency of positive post-therapy ^{131}I scans in this group of patients. Wells et al. [16] reviewed 13 studies that evaluated the frequency of positive ^{131}I post-therapy scans in patients who had negative pre-therapy radioiodine scans. The frequency of positive ^{131}I post-therapy scans ranged from 25 to 94 %, and for the composite results of all these articles, 61 % (200/329) of the patients had a positive ^{131}I post-therapy scan.

With the initial data indicating that ^{124}I PET scans are superior to ^{131}I planar scans, the question is whether or not ^{124}I PET scans could better differentiate which patients would have uptake on the post-therapy ^{131}I scan, thereby providing a potentially better prediction of those patients who may benefit from a "blind treatment." Unfortunately, preliminary data from Freudenberg et al. [17] and Chennupati et al. [18] might suggest otherwise. In six of seven patients with disseminated iodine-avid lung metastases, Freudenberg et al. [17] reported that the ^{131}I post-therapy scan was positive despite the ^{124}I PET scan being negative. However, Freudenberg et al. used a prescribed activity of ^{124}I of only 24 ± 2 MBq (0.65 mCi). In five of seven patients, Chennupati et al. [18] reported that the ^{131}I post-therapy scan was positive despite the ^{124}I PET scan being negative. In this study the prescribed activity of ^{124}I was only 63 MBq (1.7 mCi). An update by Khorjekar et al. [19] reported that in 12 patients with negative diagnostic ^{124}I PET scan, 10 patients had positive post-^{131}I therapy scans. This report suggests that a negative ^{124}I PET scan will not be any better than ^{131}I imaging in determining (1) if metastatic differentiated thyroid cancer foci are radioiodine avid, (2) whether or not a post-therapy scan after an ^{131}I "blind treatment" will be positive, or (3) whether or not a therapy with ^{131}I will alter patient . However, higher prescribed actitivies of ^{124}I may be necessary.

^{124}I PET Lesion Detection to Evaluate Patient Preparation

^{124}I PET scans have already been used to evaluate other issues involving DTC and one example is the evaluation of the effectiveness of patient preparation (e.g., THW versus

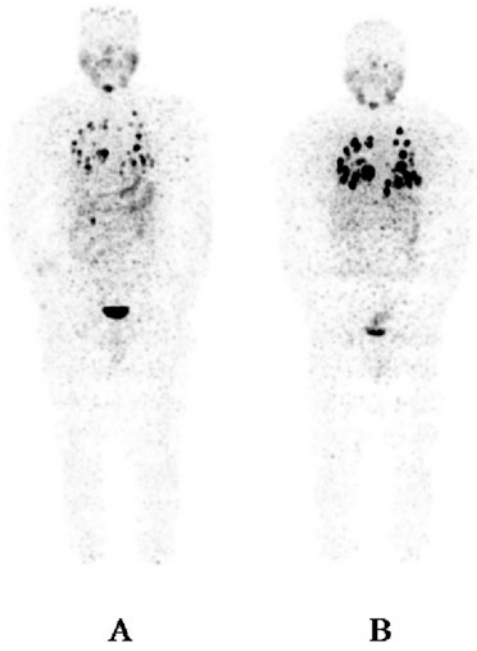

Fig. 103.6 This is a 47-year-old male with metastatic thyroid carcinoma. Image (**a**) is the maximum intensity projection image obtained 48 h after the administration of ~33.3 MBq (0.9 mCi) of ^{124}I after the patient was prepared with two intramuscular injections of 0.9 mg of recombinant human thyroid-stimulating hormone. Image (**b**) is also the anterior maximum intensity projection image obtained 48 h after the administration of ~33.3 MBq (0.9 mCi) of ^{124}I after the patient was prepared with thyroid hormone withdrawal. This image was obtained 1 week after image (**a**). All imaging parameters were the same. More intense foci of ^{124}I are observed in this patient after preparation with thyroid hormone withdrawal. However, further evaluation is warranted (Images reproduced with permission from Keystone Press, Inc)

rhTSH injection) in the detection of metastatic foci in patients in whom metastatic DTC is suspected. Freudenberg et al. [20] using ^{124}I PET-CT scans retrospectively evaluated 63 patients, of whom 27 were prepared using recombinant human thyroid-stimulating hormone (rhTSH) and 36 by thyroid hormone withdrawal (THW). Their data suggested that preparation with rhTSH resulted in a lower radiation absorbed dose to DTC metastases than preparation with THW, but their data was not statistically significant. In 40 patients of whom 24 patients were prepared with rhTSH injections and 16 were prepared with THW, Van Nostrand et al. [21] using ^{124}I PET scans reported data favoring THW relative to rhTSH injection. Two patients had ^{124}I PET imaging performed after preparation with both THW and rhTSH injections. For both of these patients, the THW preparation demonstrated more metastatic lesions (see Fig. 103.6). A full discussion of which method of preparation is superior in the management of patients with metastatic DTC is beyond the scope of this chapter, but rather these studies demonstrate the potential use of ^{124}I PET scans in the evaluation of other controversial aspects of the management of DTC.

Dosimetry

Overview

Dosimetry is essentially the calculation of radiation absorbed dose, which is defined in terms of the energy imparted by radioactive substances divided by the mass of the target tissue and can be used to help determine the likely damage to tissue. More specifically, absorbed dose has been shown to correlate to damage in normal organs [22, 23], which is the main reason that accurate calculation of absorbed dose is fundamentally important in therapeutic nuclear medicine. Used prospectively, dosimetry can enable the optimization of treatment by maximizing the amount of radioactive substance to administer to a patient while still adhering to constraints of toxicity. Used retrospectively, dosimetry can establish tumor dose-response relationships [24–26].

^{124}I-based dosimetry does not differ from dosimetry for any other radiopharmaceutical. That is, the same principles still apply and the different techniques are the same. The two most common methods are (a) the absorbed fraction methodology and (b) three-dimensional personalized dosimetry. A brief review of these two methods follows.

In therapeutic nuclear medicine, in the ubiquitous classic "absorbed fraction" paradigm, the dose to a target region (typically an organ), used to ascertain likely toxicity to that organ, consists of dose contributions from all organs in the body, which take up activity and whose emissions may deposit energy in the target organ. The basic equation that describes this approach is the following [MIRD] (Medical Internal Radiation Dose) (http://www.nndc.bnl.gov/mird/):

$$D_t = \sum_s \frac{A_s \cdot \Delta \cdot \phi_{t \leftarrow s}}{m_t}$$

That is, the absorbed dose in a target region (usually an organ) is equal to the sum of the dose contributions from all source organs in the body, where the major source organ contributor is usually the target organ itself (self-dose contribution). Each contribution is equal to the time-integrated activity (TIA, or number of decays), $\tilde{A}s$, in the source multiplied by the energy per decay, Δ, (isotope dependent) multiplied by the absorbed fraction of emitted energy, ϕ, that originates in the source organ and is deposited in the target organ and divided by the target mass *mt*. In order to facilitate the application of this formula, a first-order anthropomorphic phantom model was developed by Cristy and Eckerman [27], and a library of results were generated by the MIRD committee which incorporates the mass, absorbed fraction, and energy per decay parameters into a single parameter referred to as the S-factor that simplifies the equation above:

$$D_t = \sum_s \tilde{A}_s \cdot S_{t \leftarrow s}$$

This phantom model allowed the creation of a library of data from which dosimetric calculations could be made simply by knowing the number of decays (TIA) in each organ ($\tilde{A}s$). A software program which exploits this library and is the most common means for estimating dose is OLINDA/EXM [28]. Note that typically for DTC, the therapeutic isotope is ^{131}I; therefore, the S-values, ϕ and Δ, pertain to that isotope.

The number of decays, or time-integrated activity, is determined by integrating the activity in an organ over time, as the name implies. Practically, this is realized by (a) imaging, (b) quantifying the activity in a particular region (organ) at several time points, (c) adjusting the activity to account for the half-life difference between ^{124}I and ^{131}I, (d) graphing the activity as a function of time, and (e) integrating the activity by computing the area under the curve fit to an a priori function (or the area under the curve formed by linearly connecting the different points followed by an exponentially decaying tail). That several time points are necessary follows from the fact that the activity is redistributing between organs over time as it decays. This redistribution occurs predominantly at earlier time points, although these can still be on the order of days as is the case for radioiodine. Clearly, more time points will provide a more accurate fit for the integration; however, the time and cost of imaging limit the number of sessions. The typical range for radioiodine dosimetry is three to five images, but a method exists that uses only two time points, which is relatively reliable [29].

Just as clearly, accurate quantification of the activity is essential for reliable dosimetry. From this standpoint, the advantage of ^{124}I PET imaging over ^{131}I planar or even SPECT imaging is unequivocal. As a rule of thumb, the relative merits of the imaging modalities vis-à-vis detection discussed in the previous section translate to an even greater degree for quantification. In particular, the issues with quantitation derived from planar imaging have been discussed at length [30, 31], and no matter the various scatter and attenuation corrections, two-dimensional dosimetry is approximate at best and subject to large errors. Consequently, results published using absorbed dose values derived from two-dimensional dosimetry have arguably done more harm than good in establishing confidence in dosimetry-based treatment planning.

Once the TIAs for the different organs have been established, it becomes a simple matter of converting the TIAs to absorbed dose either by using the OLINDA/EXM software or by applying the S-values directly. The advantage of such a method is its ease of use; the disadvantages lie in that the phantoms used for deriving the S-values may differ significantly in anatomy from the individual patients. Moreover, the S-values only exist for normal organs, not tumors. A spherical tumor model does exist within OLINDA/EXM, but it does not allow for tumor heterogeneity of shape or uptake and only calculates dose from the activity within the tumor, neglecting the contribution from activity in the surrounding tissues. As our understanding of dosimetry evolves, the disadvantage of the lack of versatility in the tumor model becomes increasingly clear; it is becoming more apparent that tumor response to dose depends on a variety of different factors and parameters, including dose rate and heterogeneity of dose, which are not accounted for in an absorbed fraction method which only provides the mean absorbed dose.

The alternative to the absorbed fraction method is personalized three-dimensional dosimetry, either using Monte Carlo simulations directly or via point kernel methods. These simulate the decay of activity in the patient's body using the patient's own CT and emission (PET or SPECT) images by tracking each decaying particle according to the probabilities that it will interact in a variety of different possible ways with the matter it is traversing. The Monte Carlo programs are so named because they figuratively "roll the dice" to determine the direction, energy deposition, and secondary particle creation that each decaying radionuclide will take. While this method is not accurate for individual particles, given a statistically large number of events as is the case for the number of decaying radionuclides in therapeutic nuclear medicine, the macroscopic results are accurate to within a few percentage points. Several points are worthy of note regarding these computer models: (1) while the number of events simulated is generally fairly large (one to ten million is a typical range), it is still small compared to the number of decaying particles in a patient (up to 10^{12}–10^{15} for a whole-body radioiodine treatment) and (2) such simulations are the basis for establishing the S-values used in the absorbed fraction methodology.

The energy deposited by the various decaying particles is collected in a three-dimensional matrix of voxels (volume elements) in which the patient has been segmented using the CT images and then converted to radiation dose on a voxel as well as an organ level. Several such personalized dosimetry codes exist including 3D-ID [32], 3D-RD [33], RMDP [34], Oedipe [35], FLUKA [36], and VoxelDose [37], among others. The advantages of Monte Carlo are obvious: a greater personal accuracy and the ability to incorporate tumor dosimetry and heterogeneities at the voxel level into the calculations as well as display result in a more elaborate manner such as with dose-volume histograms, for example. One disadvantage lies in the time necessary to perform the Monte Carlo analysis, on the order of hours for each simulation depending on the computer hardware.

3D-ID

3D-ID (3D internal dosimetry), the earliest 3D imaging-based targeted radionuclide dosimetry package described in the literature, was heavily influenced by treatment planning techniques developed for external radiotherapy treatment planning [32]. It has been used to examine the impact of different radionuclides on the dose distribution, given a fixed cumulated activity distribution. In particular, 3D-ID has been used in thyroid cancer patients using ^{124}I PET imaging data along with CT images for radioiodine tumor dosimetry [38]; this study demonstrated use of sequential PET image studies that were co-registered across time and integrated, voxel-by-voxel, to provide a 3-D cumulated activity image used in the tumor dosimetry calculation. The same data set and general approach were also used to perform normal organ dosimetry [39]. A next-generation version of 3D-ID, named 3D-RD, has been developed that incorporates radiobiological modeling, i.e., not just simply the radiation dose or energy deposition but also the response of the tissue to this insult.

Radiobiological Modeling

Radiobiological modeling was introduced into the 3D-ID (which subsequently became known as 3D-RD) analysis by incorporating models derived from the linear-quadratic model of cell response to radiation. Specifically, the surviving fraction of cells (SF) measured in vitro in response to varying quantities of single fractions of external radiation, D, is given by the equation:

$$\mathrm{SF} = e^{-\alpha D - \beta D^2}$$

where α and β are the linear and quadratic radiobiological coefficients, respectively. The biological effective dose (BED) is the equivalent absorbed dose delivered at a low dose rate; [40] this concept is given mathematically by

$$\alpha \mathrm{BED} = \alpha D + \beta D^2$$

Thus for low dose rates, the BED and the absorbed dose are similar, while for higher dose rates, the BED grows much larger than the absorbed dose. That this is a relevant biological quantity has been justified by the BED-response correlations established for normal organs [19, 20]. Note that according to the linear-quadratic model, cell death is associated with double-strand DNA breaking. The quadratic term relates to a double-strand break brought about by two different events separated in time as opposed to the single-event double-strand break represented by the linear term. Therefore, a repair mechanism was modeled into the BED formulation, the so-called Lea-Catcheside factor G [41], such that the equation for the BED becomes

$$\mathrm{BED} = D\left(1 + \frac{G(\infty)}{\alpha / \beta} \cdot D\right)$$

The equivalent uniform dose (EUD) is an attempt to give a representative single dose value for a heterogeneous region or organ. This concept is also based on the linear-quadratic response and is formulated thusly

$$e^{-\alpha EUD} = \frac{1}{N}\sum_{N}^{i=1} e^{-\alpha D_i - \beta D_i^2}$$

That is, the EUD is the single BED value which every voxel in a region would have in order to have the same surviving fraction of cells as the measured heterogeneous dose distribution [42]:

$$EUD = -\frac{1}{\alpha}\ln\left(\sum_{N}^{i=1}\frac{e^{-\alpha BED_i}}{N}\right)$$

To implement these models, absorbed dose rate images are calculated for each time point rather than the integrated absorbed dose from a cumulated activity map.

Assuming an exponential repair process, a BED value can be generated for each voxel, either by using a formula derived for a specific exponential functional fit [43, 44] or numerically using an algorithm [45]; subsequently, an EUD value for a particular user-defined volume can also be calculated [33].

Real-Time 3D-RD Calculation and Comparison with Conventional Dosimetry

As an example, 3D-RD was used prospectively for the planning of an ^{131}I therapy for an 11-year-old girl, who presented post-thyroidectomy with metastatic papillary carcinoma based on ^{124}I imaging [46]. In this case ^{124}I was chosen since a diagnostic quantity of ^{131}I had been administered at a different institution a week prior, of which the patient still retained a significant quantity. As previously discussed, PET utilizes coincidence photons from the positron-electron annihilation event, which are essentially unaffected by the additional emissions from ^{131}I. More precisely, the false coincidence rate from single scattered photons from the 637-keV gamma emission that occurs in about 7 % of the ^{131}I decays combining with one of the two 511-keV photons from ^{124}I decay was assumed to be negligible. The patient presented with radioiodine-avid bilateral temporal lobe lesions along with diffuse lung metastases and a serum thyroglobulin concentration of 9,553 ng/ml. Pulmonary function tests indicated both obstructive and restrictive lung defects. The real-time aspect of the 3D-RD calculations took advantage of the 3D-RD software package design that allows dose calculations to start without the need for the complete temporal data set. This was accomplished by calculating the dose rate

obtained from each scan at each time point and then integrating these over time after the last scan had been collected and processed. In this way, the time-intensive Monte Carlo calculations were performed during the interval between image acquisitions and the more rapid integration over time was performed on the dose rate images. The disease-laden lungs were dose limiting in this case and treatment planning was designed to identify the administered activity that would deliver no more than 27 Gy to the entire lungs (including tumor). The administered activity corresponding to this limit was 5.11 GBq.

Recognizing that most voxels are likely a combination of tumor and normal lung tissue due to the disseminated nature of the metastases, an effort was made to identify "tumor" vs "normal lung" voxels. Segmentation based on activity uptake at 24 h was applied; voxels with activity >30 mBq/voxel were considered tumor, the rest normal lung tissue. Discrimination by density, determined by converting CT values as used in a previous 3D-RD calculation, and clearance rate did not provide as good and consistent a tumor delineation although there was a great degree of overlap between all the approaches considered.

The voxel-averaged BED to lung voxels identified as tumor was 43.2 Gy. Accounting for the spatial non-uniformity of the absorbed dose to tumor gave an EUD of 23 Gy. The BED values for the brain lesions were 1,220 and 142 Gy; the corresponding EUD values were 89.1 and 55.9 Gy. The administered activity determined using OLINDA/EXM to deliver 27 Gy to the lungs was 3.14 GBq. Retrospective analyses revealed that the difference was due to the assumption of disease-free lungs and a reference lung mass in the OLINDA/EXM calculation. No lung mass assumption was needed in the 3D-RD calculation because the density as obtained from CT is applied to the calculation which inherently accounts for target voxel mass. When the reference lung mass used in the OLINDA/EXM calculation was adjusted for the patient's total lung mass (as determined from the CT image using 3D-RD), an administered activity of 5.17 GBq was obtained.

The patient experienced no pulmonary, neurological, or other adverse clinical response to ^{131}I treatment. At 12 and 24 months of follow-up, the patient's serum thyroglobulin after comparable thyroid hormone withdrawal had declined from its pretreatment level of 9,553 ng/ml to 777 and 130 ng/ml, respectively. The patient's metastatic lesions in the left and right lobes of the brain, which initially measured 24 and 9 mm, respectively, were both undetectable on cranial MRI at 26 months after initial radioiodine therapy.

This example highlights the importance of accurate dosimetry to avoid over- or underdosing patients. The move to greater accessibility to personalized three-dimensional dosimetry falls in line with one of the stated "pillars" of the NIH mission. In this case, the ability to move to a diagnostic imaging agent with a different, more specific, imaging modality was critical to the quick implementation of the diagnostic dosing. Waiting for the previously administered diagnostic ^{131}I to clear would have delayed treatment or necessitated a more ad hoc determination of therapeutic administered activity.

More recently, Khorjekar et al. [47] used ^{124}I and the 3DRD software discussed above to calculate the radiation absorbed dose to metastatic foci and compared the change in size of pulmonary metastases on computer tomography to the calculated radiation dose delivered in 15 pulmonary lesions in 3 patients. The calculated EUD in Gy correlated with the clinical response. Based on a logistic regression model, an EUD score of >8 predicted a combined outcome of stable disease, partial response, and clinical response versus progression. The preliminary data suggest that the calculated EUD has potential for helping to determine which lesions may respond to various amounts of prescribed activity of ^{131}I.

Utility of Organ Dosimetry: Salivary Gland Toxicity

Radiopharmaceutical therapy using ^{131}I is the treatment of choice for differentiated thyroid carcinoma of papillary and follicular origin because the ^{131}I naturally targets the thyroid tumors and thyroid remnants through the sodium-iodine symporter mechanism. However, radioiodine can also concentrate in the parotid and submandibular salivary glands, although not to any noticeable extent in the sublingual salivary glands [48]. Radioiodine activity dependent damage to the salivary parenchyma as a result of ^{131}I radiation has been reported, consequently resulting in, *inter alia*, sialadenitis and xerostomia. These conditions in turn can induce dysphagia, infectious diseases of the oral and pharyngeal mucosa, and dental and periodontal diseases. Radiation-induced salivary gland toxicity is a serious issue that affects the patients' health-related quality of life significantly [49, 50].

Normal organ toxicity from radiopharmaceutical therapy has been traditionally correlated with absorbed dose, most often in the form of a maximum tolerated dose. However, to date, no correlation between any dosimetric quantity and clinically observed toxicity has been established for the salivary gland toxicity resulting from ^{131}I therapy for thyroid cancer [51]. In particular, a study using ^{131}I, gamma camera imaging, and volume estimations primarily from ultrasound imaging resulted in absorbed dose values five to ten times too low to satisfactorily explain the observed glandular radiation damages in radioiodine therapy [52]. The dosimetry in this case was based on standard MIRD methodology of absorbed fractions and, therefore, assumed homogenous distribution of activity in the salivary glands.

An ^{124}I PET-based salivary gland dosimetry study was undertaken with the goal of reconciling dosimetry and observed clinical toxicities; however, that study also calculated low absorbed dose results comparable to those from the previous study, and the discrepancy between absorbed and observed toxicity remained unresolved [53]. In a further study, the salivary gland dosimetry was performed using 3D-RD on a similar patient data set using ^{124}I with the idea that (a) the BED may correlate better with toxicity, (b) external factors such as thyroid remnants and lymph node metastases with high uptake proximal to the salivary glands may have a significant contribution to the absorbed dose of the salivary glands, or (c) voxelized results may lead to improved identification of the local distribution of the absorbed dose [54]. The results to date have shown that regions of high uptake external to the salivary gland can increase the total absorbed dose by a factor of two; however the contribution from this effect and the dose rate effect modeled by the BED are insufficient to explain the observed clinical toxicities. This suggests that the third proposed possibility, a more accurate voxelized analysis may be necessary; this corresponds to a localization of the activity within the gland itself, thus resulting in regions of higher uptake and dose, so-called hot spots. Previously published results have established that iodine is concentrated into the epithelium of the salivary glands' intralobular ducts before being released into the saliva, which provide the anatomical reference for the region of higher uptake [55, 56]. However, there are technical difficulties associated with voxelized quantification of salivary gland uptake, which must be taken into account. One is common to all small volumes, including small tumors and the salivary glands as a whole: the partial volume effect (PVE), also known as the "spill-out" effect, which is essentially the accuracy at which the activity can be localized in a volume. For all volumes containing activity, a certain quantity of activity at the edge of the volume will be measured outside of the volume. As the size of the VOIs decrease, the ratio of surface to volume decreases resulting in a proportionately larger amount of activity, which is mislocated. This effect has been quantified for volumes the size of salivary glands by Jentzen et al. [57, 58] and Teo et al. [59]; however, these adjustments (known as recovery coefficients) assume a homogenous distribution of activity, which enables accurate whole gland (or tumor) dosimetry, but defeats the objective of accurate voxelized dosimetry.

A second issue more specific to the salivary glands, and another controversial one, is the effect of sialogogues, including the use of lemon candies, on the uptake and retention of activity in the salivary glands. Nakada et al. [60] and Jentzen et al. [61] have claimed that the use of lemon juice increases absorbed dose to the salivary glands due to the increased salivary flow, while Van Nostrand et al. [62] demonstrated that if sialogogues are given as frequently as 20–40 min rather than every 2–3 h as evaluated by Nakada et al., the radiation absorbed dose to the salivary glands may potentially be significantly reduced. Two possible reasons for these different results may have to do with the frequency of administration of sialogogues and the measurements of radioactivity in the salivary glands at periodic intervals of hours vs minutes. What is known is that there is a great deal of uncertainty in the absorbed dose and activity uptake measurements due to the rapid and extreme fluctuations in the quantity of radioiodine in the salivary glands from salivation and uptake. From this standpoint the approach by van Nostrand et al. [60] which monitors the activity on a much shorter time scale (minute-by-minute) appears to be more reliable and may prove to be necessary for dosimetry as well.

Therapy

^{124}I as an alternative to ^{131}I for therapy of DTC was first proposed in 1954 by Philips et al. [63]. They argued that the uptake of iodine in sites of thyroid cancer is nonuniform with reduced uptake of radioiodine in areas as large as 1–5 mm. The β particles from ^{131}I have a maximum range of only about 2 mm with about half of them traveling only about 0.2 mm. By comparison, the β particles from ^{124}I are not only more energetic and therefore more penetrating, but the decay is also accompanied by a greater abundance of x-rays and higher energy γ-rays (see Fig. 103.1). Furthermore, ^{124}I has a reasonable physical half-life, namely, 4.18 days (see Table 103.1), and all of these factors may result in ^{124}I being a superior radioisotope for therapy in selected situations. In 1960, Phillips et al. [1] reported the first patient treated with ^{124}I, and they reported a partial response. Goolden et al. [64] treated three patients with thyroid cancer with ^{124}I to ablate residual thyroid tissue remaining after a hemithyroidectomy. The prescribed activities were 1.11 GBq (30 mCi) for the first two patients and 0.72 GBq (19.5) mCi for the third patient. Successful ablation was achieved in the first two patients. However, it was most likely that ^{124}I as a therapeutic radioisotope of iodine for the therapy of DTC did not become routine because of availability, cost, and little initial data to support a significant advantage over ^{131}I. Although it may be time to reconsider ^{124}I as a therapeutic radioisotope of iodine, perhaps even as a "cocktail" along with ^{131}I, for DTC, the three original limitations remain – availability, cost, and a lack of documentation of a significant advantage over ^{131}I.

Future

For differentiated thyroid cancer, ^{124}I holds significant promise for lesion detection as well as lesion, organ, and whole-body dosimetry, and ^{124}I PET-CT may one day be available

for routine clinical imaging and dosimetry. However, it is difficult to predict when that will occur in the United States and whether or not ^{124}I PET will completely replace ^{131}I and/or ^{123}I for either imaging or dosimetry for one major reason. To our knowledge, ^{124}I cannot be patented, which is a major obstacle for funding the clinical studies and other regulatory requirements needed to obtain approval by the Food and Drug Administration (FDA) in the United States. Thus, there is little incentive for any company to invest the time, money, and resources to develop and submit a new drug application (NDA) to the FDA when upon that NDA's approval any company would be able to market ^{124}I without having shared in any of the development costs.

Although cost and availability are two disadvantages of ^{124}I as noted above, one author (dvn) believes that once ^{124}I is approved by the FDA, third-party payers will begin to reimburse for ^{124}I PET-CT scan in selected patients, and then as volumes increase, availability will increase, and the cost will decrease.

Summary

In summary, ^{124}I is a promising isotope of radioiodine that will improve the diagnostic imaging of differentiated thyroid cancer by allowing PET-CT imaging, which in turn will improve resolution, offer tomographic images, and permit fusing of the PET images with CT and/or MR images. In addition, ^{124}I will help determine more accurately and reproducibly estimates of radiation absorbed doses to thyroid cancer cells and other organs of the body for ^{131}I treatments.

Acknowledgments Studies evaluating ^{124}I performed at MedStar Washington Hospital Center were supported by grants from the Latham Fund, Genzyme Corporation, IBA Corporation, and grateful patients.

References

1. Phillips A, Haybittle J, Newbery G. Use of ^{124}I for the treatment of carcinoma of the thyroid. Acta Unio Int Contra Cancrum. 1960;16:1434–8.
2. Rhodes B, Wagner H, Gerald M. Iodine-123: development and usefulness of a new radiopharmaceutical. Isot Radiat Technol. 1967;4:275–80.
3. Freudenberg LS, Antoch G, Jentzen W, et al. Value of ^{124}I-PET/CT in staging of patients with differentiated thyroid cancer. Eur Radiol. 2004;14:2092–8.
4. Rault E, Vandenberghe S, Holen R, Beenhouwer J, Staelens S, Lemahieu I. Comparison of image quality of different iodine isotopes (^{123}I, ^{124}I, and ^{131}I). Cancer Biother Radiopharm. 2007;22:423–30.
5. Freudenberg L, Jentzen W, Sahl A, Bockishc A, Rosenbaum-Krumme S. Clinical applications of ^{124}I PET-CT in patients with differentiated thyroid cancer. Eur J Nucl Med Mol Imaging. 2011;38(Suppl):S48–56.
6. Phan H, Jager P, Paans A, et al. The diagnostic value of ^{124}I-PET in patients with differentiated thyroid cancer. Eur J Nucl Med Mol Imaging. 2008;35:958–65.
7. Capoccetti F, Criscuoli B, Rossi G, Rerretti F, Manni C, Brianzoni E. The effectiveness of ^{124}I PET/CT in patients with differentiated thyroid cancer. Q J Nucl Med Mol Imaging. 2009;53:536–45.
8. Van Nostrand D, Moreau S, Bandaru V, Atkins A, Chennupati S, Mete M, Burman K, Wartofsky L. ^{124}I positron emission tomography versus ^{131}I planar imaging in the identification of residual thyroid tissue and/or metastasis in patients who have well-differentiated thyroid cancer. Thyroid. 2010;20:879–83.
9. Atkins F, Van Nostrand D, Moreau S, et al. Comparison of the blood biokinetics of ^{124}I and ^{131}I in patients with well-differentiated thyroid cancer (WDTC). J Nucl Med. 2008;49(Suppl):323.
10. Lambrecht R, Sajjad M, Qureshi M, Al-Yanbawi S. Production of iodine-124. J Radioanal Nucl Chem Lett. 1988;127:143–50.
11. Sharma H, Zweit J, Downey S, et al. Production of ^{124}I for positron emission tomography. J Label Compd Rad. 1988;26:165–7.
12. Firouzbakht M, Schlyer D, Finn R, et al. Iodine-124 production: excitation functions for the ^{124}Te(d,2n)^{124}I and ^{124}Te(d,3n)^{123}I reactions from 7 to 24 MeV. Nucl Instrum Methods B. 1993;79:909–10.
13. Khorjekar G, Van Nostrand D, Kharazi P, Moreau S, Atkins F, Chennupati S, Mete M, Burman K, Wartofsky L. ^{124}I versus ^{131}I in the identification of functioning residual thyroid tissue and/or metastases in patients with differentiated thyroid cancer: update of initial report. J Nucl Med. 2011;52(Suppl):1295.
14. Abdul-Fatah S, Zamburlini M, Halders S, Brans B, Teule G, Kemerink G. Identification of a shine-through artifact in the trachea with ^{124}I PET/CT. J Nucl Med. 2009;50:909–11.
15. Nagarajah J, Jentzen W, Hartung V, Rosenbaum-Krumme S, Mikat C, Heusner Till A, Antoch G, Bockisch A, Stahl A. Diagnosis and dosimetry in differentiated thyroid carcinoma using ^{124}I PET: comparison of PET/MRI vs PET/CT of the neck. Eur J Nucl Med Mol Imaging. 2011;38:1862–8.
16. Wells K, Moreau S, Shin YR, Van Nostrand D, Burman K, Wartofsky L. Positive (+) post-treatment (tx) scans after the radioiodine (RAI) tx of patients who have well-differentiated thyroid cancer (WDTC), positive serum thyroglobulin levels (TG+), and negative diagnostic (dx) RAI whole body scans (WBS-): predictive values and frequency. J Nucl Med. 2008;49(Suppl):238P.
17. Freudenberg L, Jentzen W, Muller S, Bockisch. Disseminated iodine-avid lung metastases in differentiated thyroid cancer: a challenge to ^{124}I PET. Eur J Nucl Med Mol Imaging. 2008;33:502–8.
18. Chennupati S, Bandaru VV, Prasad K, Van Nostrand D. Do negative diagnostic ^{131}I and ^{124}I scans exclude ^{131}I as a treatment option in patients with positive thyroglobulin levels? J Nucl Med. 2009;50(Suppl):343P.
19. Khorjekar GR, Van Nostrand D, Garcia C, O'Neil J, Moreau S, Atkins FB, Mete M, Orquiza MH, Burman K, Wartofsky L. Do Negative ^{124}I Pre-therapy Positron Emission Tomography Scans in Patients with Elevated Serum Thyroglobulin Levels Predict Negative ^{131}I Post-therapy Scans? Thyroid. 2014;24;1394–99.
20. Freudenberg LS, Jentzen W, Petrich T, et al. Lesion dose in differentiated thyroid carcinoma metastases after rhTSH or thyroid hormone withdrawal: ^{124}I PET/CT dosimetric comparisons. Eur J Nucl Med Mol Imaging. 2010;37:2264–76.
21. Van Nostrand D, Khorjekar G, O'Neil J, Moreau S, Atkins F, Kharazi P, Mete M, Chennupati S, Burman K, Wartofsky L. Recombinant human thyroid stimulating hormone versus thyroid hormone withdrawal in the identification of metastasis in differentiated thyroid cancer with ^{131}I planar whole body and ^{124}I PET. J Nucl Med. 2012;53:359–62.
22. Barone R, Borson-Chazot F, Valkema R, Walrand S, Chauvin F, Gogou L, et al. Patient-specific dosimetry in predicting renal toxicity with ^{90}Y-DOTATOC: relevance of kidney volume and dose rate

in finding a dose-effect relationship. J Nucl Med. 2005;46 Suppl 1:99S–106.
23. Wessels BW, Konijnenberg MW, Dale RG, Breitz HB, Cremonesi M, Meredith RF, et al. MIRD pamphlet No. 20: the effect of model assumptions on kidney dosimetry and response--implications for radionuclide therapy. J Nucl Med. 2008;49:1884–99.
24. Dewaraja Y, Schipper M, Roberson P, Wilderman S, Amro H, Regan D, Koral K, Kaminski M, Avram A. ^{131}I-tositumomab radioimmunotherapy: initial tumor dose-response results using 3-dimensional dosimetry including radiobiologic modeling. J Nucl Med. 2010;51:1155–62.
25. Senthamizhchelvan S, Hobbs RF, Song H, Frey EC, Zhang Z, Armour E, Wahl RL, Loeb DM, Sgouros G. Tumor dosimetry and response for ^{153}Sm-EDTMP therapy of high-risk osteosarcoma. J Nucl Med. 2012;53:215–24.
26. Maxon HR, Thomas SR, Hertzberg VS, et al. Relation between effective radiation dose and outcome of radioiodine therapy for thyroid cancer. N Engl J Med. 1983;309:937–41.
27. Cristy M, Eckerman K. Specific absorbed fractions of energy at various ages from internal photon sources. 1987 Oak Ridge National Laboratory Report ORNL/TM-8381 V1-7.
28. Stabin M, Sparks R, Crowe E. OLINDA/EXM: the second-generation personal computer software for internal dose assessment in nuclear medicine. J Nucl Med. 2005;46:1023–7.
29. Jentzen W, Freudenberg L, Eising EG, Sonnenschein W, Knust J, Bockisch A. Optimized ^{124}I PET dosimetry protocol for radioiodine therapy of differentiated thyroid cancer. J Nucl Med. 2008;49:1017–23.
30. Flux G, Bardies M, Monsieurs M, Savolainen S, Strands SE, Lassmann M. The impact of PET and SPECT on dosimetry for targeted radionuclide therapy. Z Med Phys. 2006;16:47–59.
31. He B, Frey E. Comparison of conventional, model-based quantitative planar, and quantitative SPECT image processing methods for organ activity estimation using In-111 agents. Phys Med Biol. 2006;51:3967–81.
32. Sgouros G, Kolbert K. The three-dimensional internal dosimetry software package, 3D-ID. In: Zaidi H, Sgouros G, editors. Therapeutic applications of Monte Carlo calculations in nuclear medicine. Philadelphia: Institute of Physics; 2002. p. 249–61.
33. Prideaux A, Song H, Hobbs R, He B, Frey E, Ladenson P, Wahl R, Sgouros G. Three-dimensional radiobiologic dosimetry: application of radiobiologic modeling to patient-specific 3-dimensional imaging-based internal dosimetry. J Nucl Med. 2007;48:1008–16.
34. Guy M, Flux G, Papavasileiou P, Flower M, Ott R. RMDP: a dedicated package for ^{131}I SPECT quantification, registration and patient-specific dosimetry. Cancer Biother Radiopharm. 2003;18:61–9.
35. Franck D, de Carlan L, Pierrat N, Broggio D, Lamart S. OEDIPE: a new graphical user interface for fast construction of numerical phantoms and MCNP calculations. Radiat Prot Dosimetry. 2007;127:262–5.
36. Botta F, Mairani A, Battistoni G, Cremonesi M, Di Dia A, Fassò A, Ferrari A, Ferrari M, Paganelli G, Pedroli G, Valente M. Calculation of electron and isotopes dose point kernels with FLUKA Monte Carlo code for dosimetry in nuclear medicine therapy. Med Phys. 2011;38:3944–54.
37. Dieudonné A, Hobbs R, Bolch W, Sgouros G, Gardin I. Fine resolution voxel S-values for constructing absorbed dose distributions at variable voxel size. J Nucl Med. 2010;51:1600–7.
38. Sgouros G, Kolbert K, Sheikh A, et al. Patient-specific dosimetry for ^{131}I thyroid cancer therapy using ^{124}I PET and 3-dimensional-internal dosimetry (3D-ID) software. J Nucl Med. 2004;45:1366–72.
39. Kolbert K, Pentlow K, Pearson J, et al. Prediction of absorbed dose to normal organs in thyroid cancer patients treated with ^{131}I by use of ^{124}I PET and 3-dimensional internal dosimetry software. J Nucl Med. 2007;48:143–9.
40. Dale R. Use of the linear-quadratic radiobiological model for quantifying kidney response in targeted radiotherapy. Cancer Biother Radiopharm. 2004;19:363–70.
41. Millar WT. Application of the linear-quadratic model with incomplete repair to radionuclide directed therapy. Br J Radiol. 1991;64:242–51.
42. Niemierko A. Reporting and analyzing dose distributions: a concept of equivalent uniform dose. Med Phys. 1997;24:103–10.
43. Howell RW, Goddu SM, Rao DV. Application of the linear-quadratic model to radioimmunotherapy: further support for the advantage of longer-lived radionuclides. J Nucl Med. 1994;35:1861–9.
44. Baechler S, Hobbs R, Prideaux A, Wahl R, Sgouros G. Extension of the biological effective dose to the MIRD schema and possible implications in radionuclide therapy dosimetry. Med Phys. 2008;35:1123–34.
45. Hobbs R, Sgouros G. Calculation of the biological effective dose (BED) for piecewise defined dose-rate fits. Med Phys. 2009;36:904–7.
46. Hobbs RF, Wahl RL, Lodge MA, Javadi MS, Cho S, Chien D, Ewertz ME, Esaias CE, Ladenson PW, Sgouros G. ^{124}I PET-based 3D-RD dosimetry for pediatric thyroid cancer patient: case study for real-time patient-specific dosimetry. J Nucl Med. 2009;50:1844–7.
47. Khorjekar G, Senthamizhchelvan S, Hobbs R, Orquiza M, Atkins F, Mete M, Garcia C, Wartofsky L, Sgouros G, Van Nostrand, Douglas. Correlation of ^{124}I PET dosimetry with clinical response of ^{131}I therapy for metastatic differentiated thyroid cancer. Oral presentation presented at: The Society of Nuclear Medicine annual Meeting (2013), Vancouver, British Columbia, Canada. J Nuc Med. 2013;54(Suppl):52.
48. Zanzonico PB. Radiation dose to patients and relatives incident to ^{131}I therapy. Thyroid. 1997;7:199–204.
49. Van Nostrand D. Sialoadenitis secondary to ^{131}I therapy for well-differentiated thyroid cancer. Oral Dis. 2010;17:154–61.
50. Langendijk JA, Doornaert P, Verdonck-de Leeuw IM, Leemans CR, Aaronson NK, Slotman BJ. Impact of late treatment-related toxicity on quality of life among patients with head and neck cancer treated with radiotherapy. J Clin Oncol. 2008;26:3770–6.
51. Raza H, Khan AU, Hameed A, Khan A. Quantitative evaluation of salivary gland dysfunction after radioiodine therapy using salivary gland scintigraphy. Nucl Med Commun. 2006;27:495–9.
52. Jentzen W, Schneider E, Freudenberg L, Eising EG, Gorges R, Muller SP, et al. Relationship between cumulative radiation dose and salivary gland uptake associated with radioiodine therapy of thyroid cancer. Nucl Med Commun. 2006;27:669–76.
53. Jentzen W, Hobbs RF, Stahl A, Knust J, Sgouros G, Bockisch A. Pre-therapeutic ^{124}I PET(/CT) dosimetry confirms low average absorbed doses per administered ^{131}I activity to the salivary glands in radioiodine therapy of differentiated thyroid cancer. Eur J Nucl Med Mol Imaging. 2010;37:884–95.
54. Hobbs R, Jentzen W, Bockisch A, Sgouros G. Monte Carlo-based 3-dimensional dosimetry of salivary glands in radioiodine treatment of differentiated thyroid cancer estimated using ^{124}I PET. Q J Nucl Med Mol Imaging. 2013;57:79–91.
55. Gates GA, Work WP. Radioisotope scanning of the salivary glands. A preliminary report. Laryngoscope. 1967;77:861–75.
56. Mishkin FS. Radionuclide salivary gland imaging. Semin Nucl Med. 1981;11:258–65.
57. Jentzen W. Experimental investigation of factors affecting the absolute recovery coefficients in iodine-124 PET lesion imaging. Phys Med Biol. 2010;55:2365–98.
58. Jentzen W, Weise R, Kupferschlager J, et al. Iodine-124 PET dosimetry in differentiated thyroid cancer: recovery coefficient in

2D and 3D modes for PET(/CT) systems. Eur J Nucl Med Mol Imaging. 2008;35:611–23.
59. Teo BK, Seo Y, Bacharach SL, Carrasquillo JA, Libutti SK, Shukla H, et al. Partial-volume correction in PET: validation of an iterative postreconstruction method with phantom and patient data. J Nucl Med. 2007;48:802–10.
60. Nakada K, Ishibashi T, Takei T, et al. Does lemon candy decrease salivary gland damage after radioiodine therapy for thyroid cancer? J Nucl Med. 2005;46:261–6.
61. Jentzen W, Balschuweit D, Schmitz J, et al. The influence of saliva flow stimulation on the absorbed radiation dose to the salivary glands during radioiodine therapy of thyroid cancer using ^{124}I PET/CT imaging. Eur J Nucl Med Mol Imaging. 2010;37: 2298–306.
62. Van Nostrand D, Bandaru V, Chennupati V, Kulkarni K, Wexler J, Atkins F, Mete M, Gadwale G. Radiopharmacokinetics of radioiodine in the parotid glands after the administration of lemon juice. Thyroid. 2010;20:1113–9.
63. Phillips AF. The gamma -ray dose in carcinoma of the thyroid treated by radio-iodine. Acta Radiol. 1954;41:533–44.
64. Goolden AWG, Fowler JF, Matthews CM. Comparison of iodine 124 and iodine 131 for thyroid ablation. Br J Radiol. 1963;36:346–9.
65. Koehler L, Gagnon K, McQuarrie S, Wuest F. Iodine-124: a promising positron emitter for organic PET chemistry. Molecules. 2010;15:2686–718.
66. Hall T, Siegel M, et al. Production of ^{124}I by the deuteron bombardment of tellurium. Phys Rev. 1954;95:1208.